Article:
Cadilhac, C., Bachy, I., Forget, A. et al. (7 more authors) (2021) Excitatory granule neuron precursors orchestrate laminar localization and differentiation of cerebellar inhibitory interneuron subtypes. Cell Reports, 34 (13). 108904. ISSN 2211-1247

https://doi.org/10.1016/j.celrep.2021.108904

Cell Reports

Article

Excitatory granule neuron precursors orchestrate laminar localization and differentiation of cerebellar inhibitory interneuron subtypes

Graphical abstract

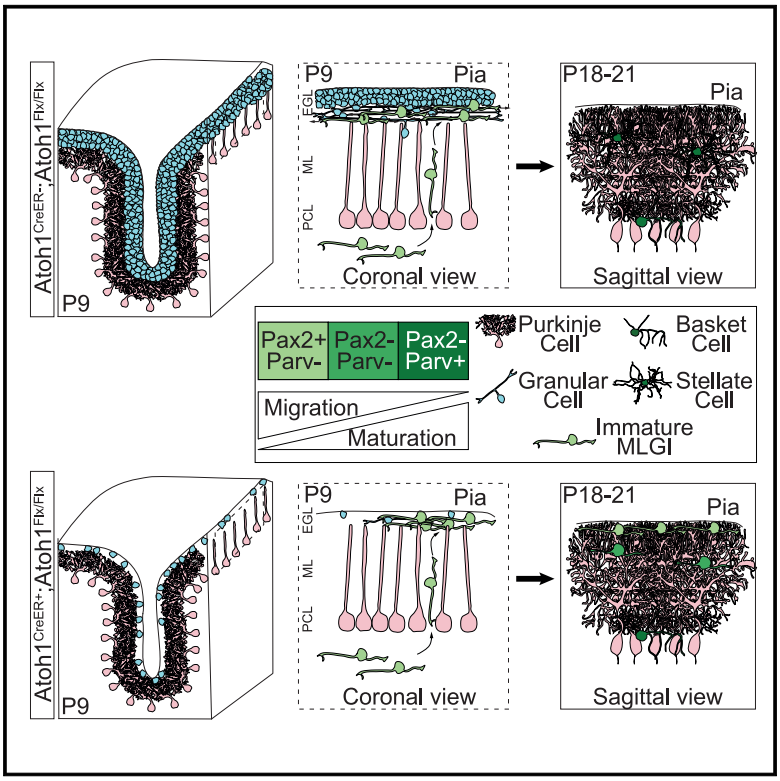

Highlights

- Basket cells and stellate cells use stereotyped migration paths in cerebellum
- Stellate cells migrate tangentially in the external granule cell layer
- Immature granule cell neurites support stellate cell tangential migration
- Genetic depletion of granule cells affects stellate cell differentiation

Authors

Christelle Cadilhac, Isabelle Bachy, Antoine Forget, ..., Patrice Mollard, Constantino Sotelo, Fabrice Ango

Correspondence

fabrice.ango@inserm.fr

In brief

Cadilhac et al. report that molecular layer GABAergic progenitors use distinct migration paths to reach their laminar position in the cerebellum where they differentiate into basket cells (BCs) and stellate cells (SCs). SCs perform an additional tangential migration step along immature granule cell neurites whose genetic depletion mainly affects SC differentiation.

Cadilhac et al., 2021, Cell Reports *34*, 108904
March 30, 2021
https://doi.org/10.1016/j.celrep.2021.108904

CellPress

Cell Reports

CellPress
OPEN ACCESS

Article

Excitatory granule neuron precursors orchestrate laminar localization and differentiation of cerebellar inhibitory interneuron subtypes

Christelle Cadilhac,[1,8] Isabelle Bachy,[1] Antoine Forget,[2,3] David J. Hodson,[4] Céline Jahannault-Talignani,[1] Andrew J. Furley,[5] Olivier Ayrault,[2,3] Patrice Mollard,[1] Constantino Sotelo,[6] and Fabrice Ango[1,7,9,*]

[1]IGF, University Montpellier, CNRS, INSERM, Montpellier, France
[2]Institut Curie, Université PSL, CNRS UMR3347, INSERM U1021, Signaling Radiobiology and Cancer, 91400 Orsay, France
[3]Université Paris-Saclay, CNRS UMR3347, INSERM U1021, Signaling Radiobiology and Cancer, 91400 Orsay, France
[4]Institute of Metabolism and Systems Research and Centre of Membrane Proteins and Receptors, University of Birmingham, Edgbaston B15 2TT, UK
[5]Department of Biomedical Science, University of Sheffield, Western Bank, Sheffield S10 2TN, UK
[6]Institut de la Vision INSERM, UMRS_U968, Paris, France
[7]INM, University Montpellier, INSERM, CNRS, Montpellier, France
[8]Present address: Department of Basic Neuroscience, University of Geneva, Geneva, Switzerland
[9]Lead contact
*Correspondence: fabrice.ango@inserm.fr
https://doi.org/10.1016/j.celrep.2021.108904

SUMMARY

GABAergic interneurons migrate long distances through stereotyped migration programs toward specific laminar positions. During their migration, GABAergic interneurons are morphologically alike but then differentiate into a rich array of interneuron subtypes critical for brain function. How interneuron subtypes acquire their final phenotypic traits remains largely unknown. Here, we show that cerebellar molecular layer GABAergic interneurons, derived from the same progenitor pool, use separate migration paths to reach their laminar position and differentiate into distinct basket cell (BC) and stellate cell (SC) GABAergic interneuron subtypes. Using two-photon live imaging, we find that SC final laminar position requires an extra step of tangential migration supported by a subpopulation of glutamatergic granule cells (GCs). Conditional depletion of GCs affects SC differentiation but does not affect BCs. Our results reveal how timely feedforward control of inhibitory interneuron migration path regulates their terminal differentiation and, thus, establishment of the local inhibitory circuit assembly.

INTRODUCTION

The large repertoire of GABAergic interneuron cell types has become increasingly central to our understanding of physiological brain functions and proper control of excitatory-inhibitory balance (Kepecs and Fishell, 2014; DeFelipe et al., 2013; Huang and Paul, 2019; Ascoli et al., 2008). Dysfunctions in inhibitory local circuit formation have been linked to several brain disorders including autism and schizophrenia (Marín, 2012). Thus, understanding the sequence of events leading to such neuronal diversity is mandatory for a complete appreciation of nervous system function.

From their last division and until they reach their final position, GABAergic interneurons undergo a long journey through diverse migratory routes. The impact of the migration path in cell fate acquisition remains unclear. Indeed, the detailed migration routes and timing of integration for a given subtype are still missing (Lim et al., 2018; Wamsley and Fishell, 2017). This is primarily due to the fact that most neurochemical markers that define interneuron classes are expressed long after they reach their homing position. Complicating matters further is the fact that genetic modification that perturbs cell specification often alters the migration process as well. In the cerebellar cortex, basket cells (BCs) and stellate cells (SCs) are the two stereotyped molecular layer GABAergic interneuron (MLGI) subtypes that derive from the same pool of PAX2 (paired box gene 2)-positive progenitors, with no genetic marker to differentiate them (Carter et al., 2018; Maricich and Herrup, 1999). The current view of cerebellar development indicates that these interneurons invade the molecular layer (ML) from postnatal day 3 (P3) to P14 in an "inside-out" manner (Yamanaka et al., 2004; Zhang and Goldman, 1996). The first neurons that reach the ML start their differentiation in close proximity to the Purkinje cell (PC) soma and give rise to the BC phenotype. The latter neurons gradually integrate into a more superficial laminar position before differentiating into SCs (Rakic, 1973). Beside the shape/size of their respective cell body, as well as dendrites and axon arborization specificities, BCs and SCs innervate separate subcellular domains of PCs. SC axons make connections with the PC dendritic domain (Ango et al., 2008) in the outer region of the ML.

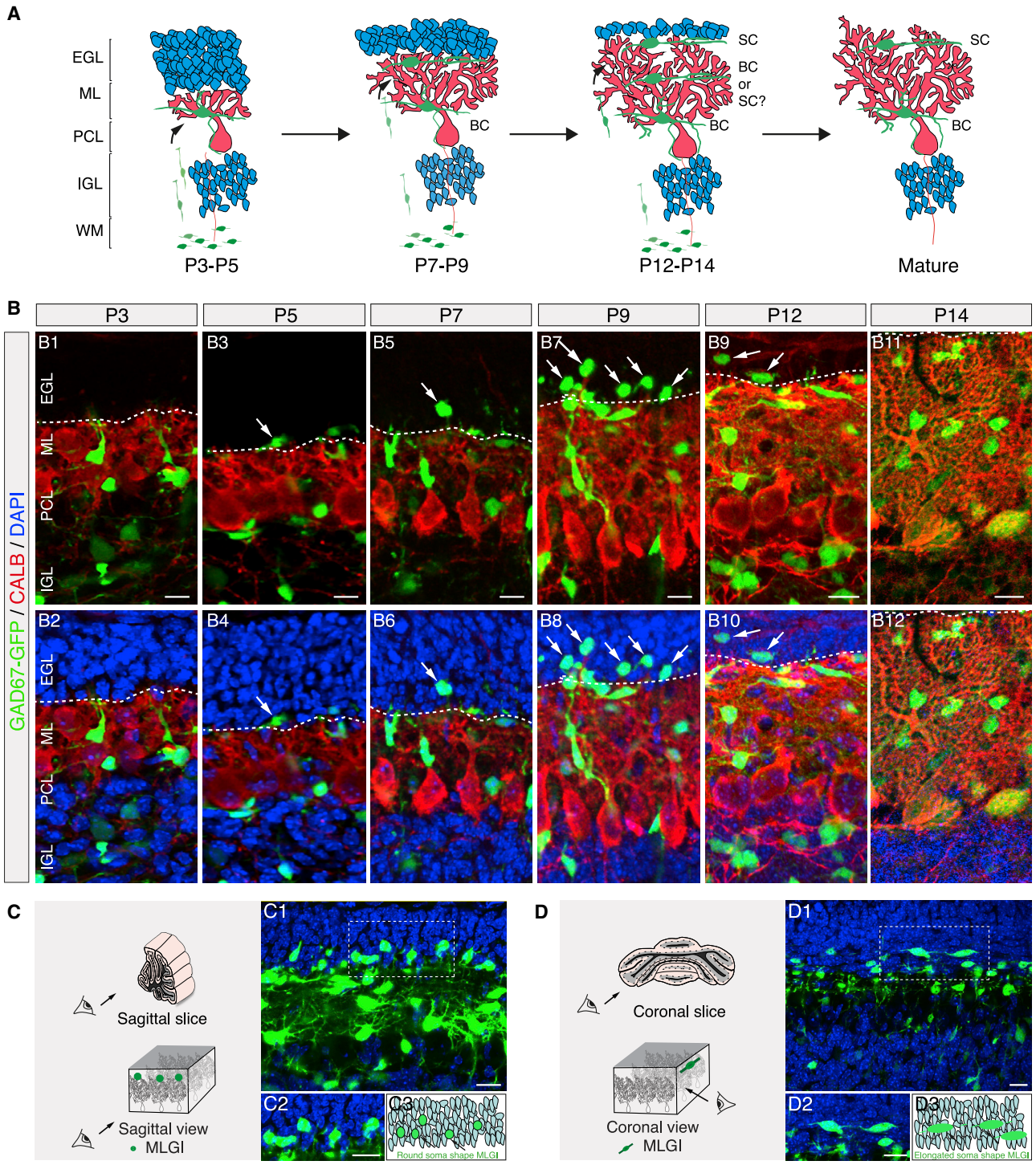

Figure 1. A proportion of immature MLGIs exhibiting migrating morphology accumulates in the EGL during cerebellar development

(A) Schematic representation of the cerebellar cortex during development showing the inside-out mode of molecular layer GABAergic interneuron (MLGI) integration. Immature interneurons settle in the ML by using several successive migration waves; at postnatal day 7 (P7), MLGIs enter the ML and start their differentiation just above Purkinje cell soma as typical basket cells (BCs). Between P9 and P14, MLGIs reach a more superficial location of the ML and differentiate as stellate cells (SCs).

(B) Confocal images of sagittal cerebellar slices of GAD67-GFP mice at P3, P5, P7, P9, P12, and P14. Between P5 and P12, a subset of MLGIs (green) accumulated into the EGL (white arrows) above Purkinje cell dendrites (Calbindin, red).

(legend continued on next page)

Conversely, BC axons target mostly PC somas and axon initial segments (AISs) by forming the pinceau synapse (Ango et al., 2004; Telley et al., 2016), providing ultrafast inhibition at AISs by ephaptic transmission (Blot and Barbour, 2014; Kole et al., 2015). However, the mechanisms that control the specific laminar position and differentiation of BCs versus SCs remain largely unknown.

Here, we combined complementary approaches to explore the mechanisms that regulate MLGI laminar position and interneuron-subtype-specific differentiation *in vivo*. We demonstrate that MLGIs use two stereotyped migration routes to reach their laminar position and differentiate respectively into BCs and SCs. Our results reveal that late-integrating MLGIs have an additional migration step in contact with the local excitatory granule cell progenitors, favoring the emergence of the specific SC subtype.

RESULTS

A subpopulation of MLGIs accumulates in the external granule cell layer (EGL) and migrates tangentially

MLGIs are present in the white matter of the cerebellar cortex from P0 and derived from PAX2-expressing precursors. Indistinguishable SC and BC precursors integrate into the ML at the same time window (Figure 1A). Therefore, we hypothesized that phenotypic differences between SCs and BCs might reflect cell-type-specific divergences during the process of their integration into ML neural circuits, possibly due to environmental factors.

Using GAD67-GFP (G42) BAC transgenic mice that reliably express GFP in MLGIs (Ango et al., 2004), we analyzed a series of fixed cerebellar sagittal slices during the MLGI integration window. We observed a fraction of GFP^+ MLGIs accumulating in the EGL, just above PC dendrites, from P5 to P14 (Figure 1B) in all the cerebellar lobes (Figures S1A and S1B). In contrast to BCs, which started their differentiation and expressed parvalbumin (PARV) in proximity to the PC soma (Figures S1D and S1E), the subset of MLGIs accumulated in the EGL expressed PAX2 with a peak in neuronal density at P9 (Figures S1D and S1E). These MLGIs displayed a round-shaped cell body in the sagittal plane (Figure 1C) and a vertically elongated soma with a thick leading process in the coronal plane (Figure 1D), highly suggestive of migrating neurons (Simat et al., 2007).

Because tangential migration of MLGIs has not been described in the mediolateral axis of the EGL (coronal plane) at postnatal stages, we initiated a series of live-imaging experiments on acute coronal and sagittal cerebellar slices by using two-photon microscopy (Figures 2A–2D; Figure S2). At P3, MLGIs entered the ML by using a radial migration step (Figure 2A; Figure S2A). After P5, we observed MLGIs entering the EGL from the ML and switching from radial to tangential migration (Figure S2B; Video S1). At P9, live imaging revealed that MLGIs located in the EGL migrate tangentially in coronal sections (Figure 2B; Figure S2A; Video S2). The tracking data showed that individual migrating cells extended a long motile leading process toward the migrating direction. All cells exhibited a saltatory movement followed by a rapid retraction of the trailing processes. To exclude the possibility that they migrate in other directions not detectable in coronal and sagittal slices, we also used flat-mount preparations from the cerebellar cortex. As shown in Figures 2C and S2A, tangentially migrating cells followed only one single axis corresponding to the mediolateral orientation of the cerebellar cortex, as previously observed in the EGL of coronal slices (Video S3), but migration was not detected in the sagittal plane (Figure S2C; Video S4). In the flat-mount preparation, a few cells with a perpendicular migration oriented toward the mediolateral axis were also observed (Figure S2A). These cells displayed a shorter migration track (Figure S2A) and were localized in the ML, just below tangentially migrating MLGIs in the EGL (Figure S3). Thus, perpendicularly migrating cells represent MLGIs that exit the EGL for their final positioning and differentiation in the sagittal plane. The proportion of neurons undergoing tangential migration in the EGL was drastically reduced around P14, which marked the end of tangential migration in cerebellar cortex (Figure 2D; Figure S2A). Migrating cells displayed an average speed of 21 μm/h (±3.3) and covered an average distance of 61.1 μm (±3.4) during the 200 min of recording at P9 (Figures 2E and 2F). At P14, MLGIs had an average speed of 9 μm/h (±0.9) and covered 17 μm (±1.1) during the recording session (Figures 2E and 2F). In conclusion, our data show that, during development, late-integrating MLGIs enter the EGL and switch from radial to tangential migration along the mediolateral axis between P5 and P14, corresponding to the SC integration window (Sudarov et al., 2011).

MLGI tangential migration is supported by premigratory granule cells in the EGL

The EGL is assumed to provide a stop signal to MLGIs (Guijarro et al., 2006) that prevents their migration in this territory. To better characterize this additional tangential migration stream during cerebellar development, we performed a new series of live-imaging experiments to demonstrate that the migration was occurring in the EGL. This time, prior to live data acquisition, P9 coronal slices were incubated in a solution of CyTRAK, a live-cell nuclear orange dye, allowing clear visualization of the densely packed granule cell nuclei and thus clear delineation of the ML/EGL border during live imaging. This experiment showed that tangential MLGI migration occurred within the EGL (Figure 3A; Video S5). The EGL is composed of two distinct regions, namely, the outer EGL (oEGL) that contains proliferating granule cell precursors and the inner EGL (iEGL) containing postmitotic differentiating granule cells extending TAG-1-positive parallel axons (Stottmann and Rivas, 1998).

(C and D) On the left of each panel, a diagram of a sagittal (C) and a coronal (D) section. At the bottom, the view angle of the 3D organization of the cerebellum. Soma of MLGI located in the EGL exhibit a round shape in the sagittal plane (C1, C2, and diagram) and a rather elongated shape with a thick leading process in the coronal plane (D1,D2, and diagram), which is highly suggestive of migrating interneurons.
Scale bars: 20 μm. EGL, external granule cell layer; PCL, Purkinje cell layer; IGL, internal granule cell layer; WM, white matter; CALB, Calbindin.
See also Figure S1.

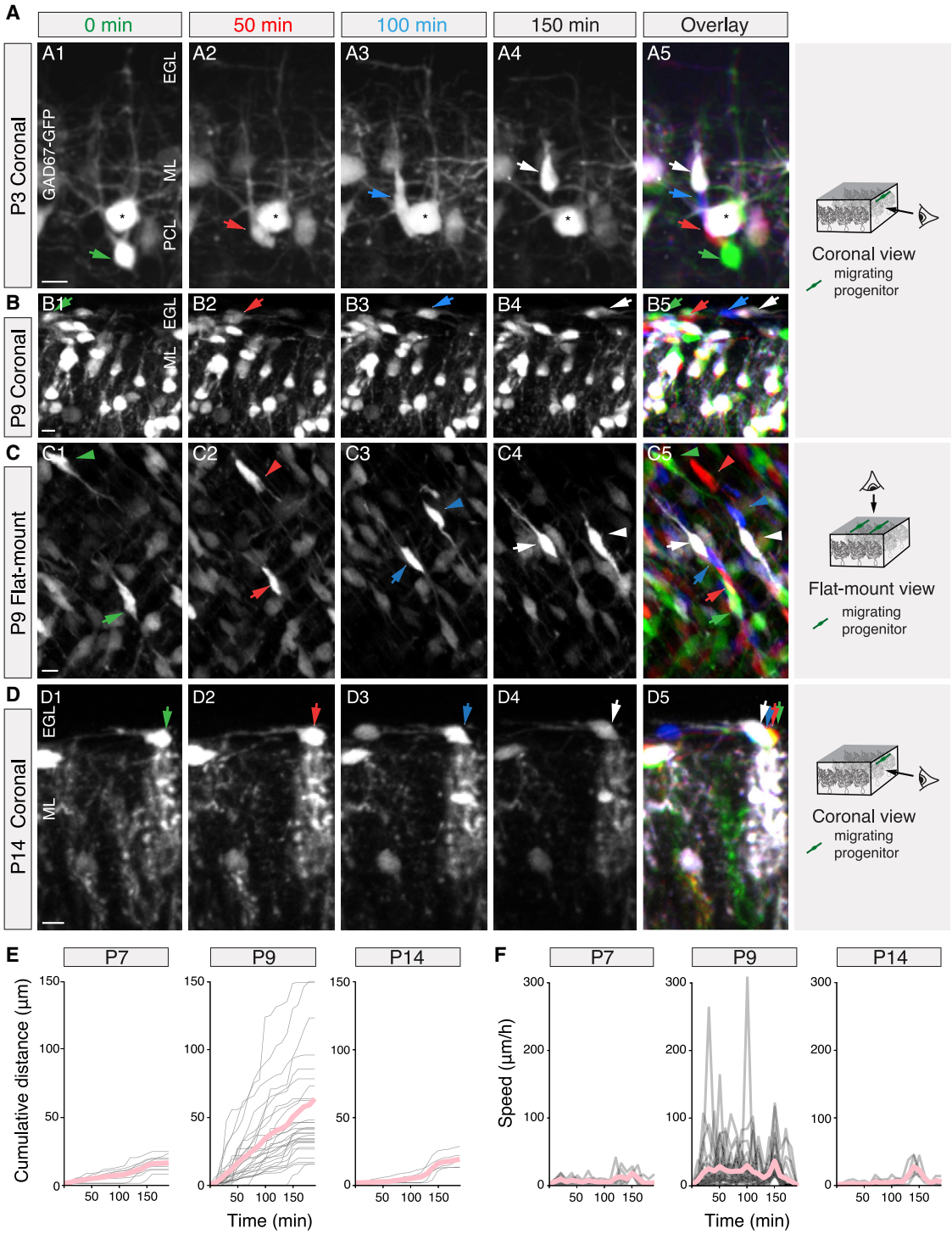

Figure 2. A subset of MLGIs accumulated in the EGL migrates tangentially

(A–D) Two-photon microscopy on acute cerebellar slices from GAD67-GFP BAC transgenic mice. The frame corresponding to the start of the time lapse (t = 0 min) is pseudo-colored in green, t = 50 min in red, t = 100 min in blue, and t = 150 min in gray. Cells are tracked at each time point (respective colored arrows and arrowheads). A diagram of the cerebellar organization in 3D and the image acquisition angle for each panel are displayed on the right side.

(A) At P3, on acute coronal slice, MLGIs use radial migration to enter the ML.

(B) At P9, in the coronal plane, MLGIs perform tangential migration at the top of the ML.

(C) At P9, on flat-mount preparation, MLGIs display a single migration orientation in the mediolateral axis in both directions.

(D) At P14, in the coronal orientation, tangentially migrating MLGIs at the top of the ML achieve their tangential migration.

(legend continued on next page)

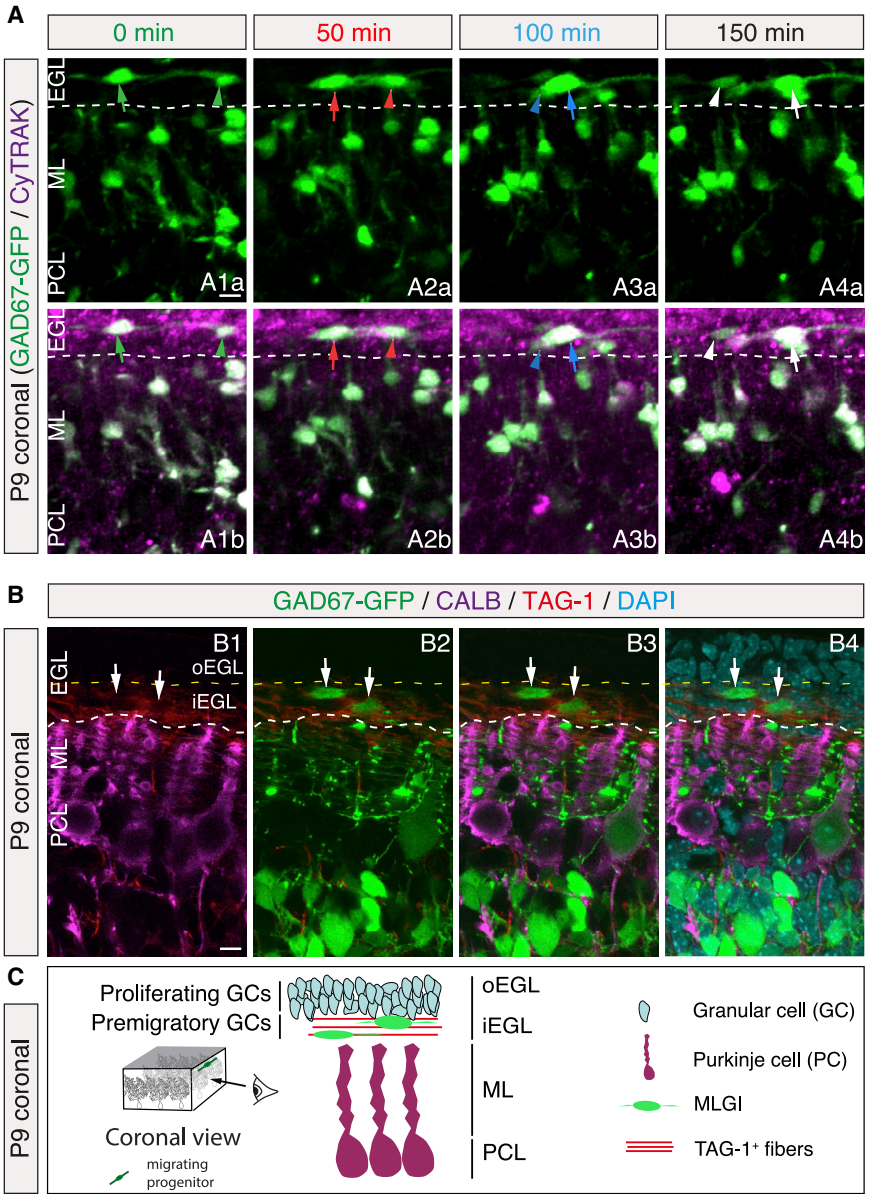

Figure 3. Tangentially migrating MLGIs are supported by TAG-1-positive granule cell axons in the EGL

(A) Live imaging on P9 acute coronal slices from GAD67-GFP BAC transgenic animals incubated with CyTRAK orange dye (magenta), a vital nuclear dye, showing MLGIs performing tangential migration in the EGL (colored arrows and arrowheads). The frame corresponding to the start of the time lapse (t = 0 min) is pseudo-colored in green, t = 50 min in red, t = 100 min, in blue and t = 150 min in gray.

(B) Confocal images of coronal sections from P9 GAD67-GFP BAC transgenic mice showing TAG-1 (red) expression restricted to the inner EGL (iEGL). Tangentially migrating MLGIs (green) are located in the TAG-1$^+$ area (white arrows).

(C) Schematic of the migrating MLGIs from the coronal view.

Scale bars: 10 μm. oEGL, outer EGL.

See also Figure S4 and Video S5.

Using a TAG-1-specific antibody, we showed that tangentially migrating MLGIs are localized in the iEGL during cerebellar development (Figures 3B and 3C; Figures S4A). To characterize the potential cellular relationship between TAG-1-positive signals from premigratory granule cells (GCs) and GFP$^+$ MLGIs, we analyzed the level of apposition between TAG-1 signals and GFP-positive MLGIs extending neurites. We observed that more than 70% of GFP-positive neurites are associated with TAG-1 signal in the EGL (Figures S4B–S4E), suggesting that parallel fibers expressing TAG-1 supported MLGI tangential migration. To test this hypothesis, we analyzed the effects of an anti-TAG-1 blocking antibody, which has been shown to disrupt physiological neurite outgrowth of GC precursors (Furley et al., 1990; Wang et al., 2011). Using time-lapse imaging in the presence of TAG-1 blocking antibody, we first observed a significant change in the orientation of MLGI migration. Indeed, acute treatment with TAG-1 blocking antibody induced MLGI dispersion in all directions, as compared to the single mediolateral orientation observed under control conditions (Figures 4A–4C; Video S6). In addition, we also observed a significant difference in the total distance traveled for the TAG-1 blocking antibody condition compared to control (61.1 ± 3.4 versus 43 ± 2.3 μm, respectively; [n = 3 and 4, respectively; $p < 0.0001$]), although the mean speed was not significantly different (17.6 ± 2.4 versus 21 ± 3.3 μm/h, respectively [n = 3 and 4, respectively; $p = 0.4302$]) (Figures 4D and 4E). Altogether, these results showed that blocking TAG-1 function in GC neurites alters MLGI migration direction and kinetics in the mediolateral axis and suggest that GC neurites in the iEGL are part of the molecular scaffolding supporting MLGI migration. Next, we asked whether TAG-1 expression per se on GC neurites also contributes to MLGI tangential migration. To

(E) Cumulative distances achieved by migrating MLGIs at P7, P9, and P14 analyzed in coronal slices. The pink curve corresponds to the mean.

(F) Quantification of instantaneous velocities of migrating MLGIs at P7, P9, and P14 analyzed in coronal slices. The pink curve corresponds to the mean.

Scale bars: 10 μm.

See also Figures S2 and S3 and Videos S2, S3, and S4.

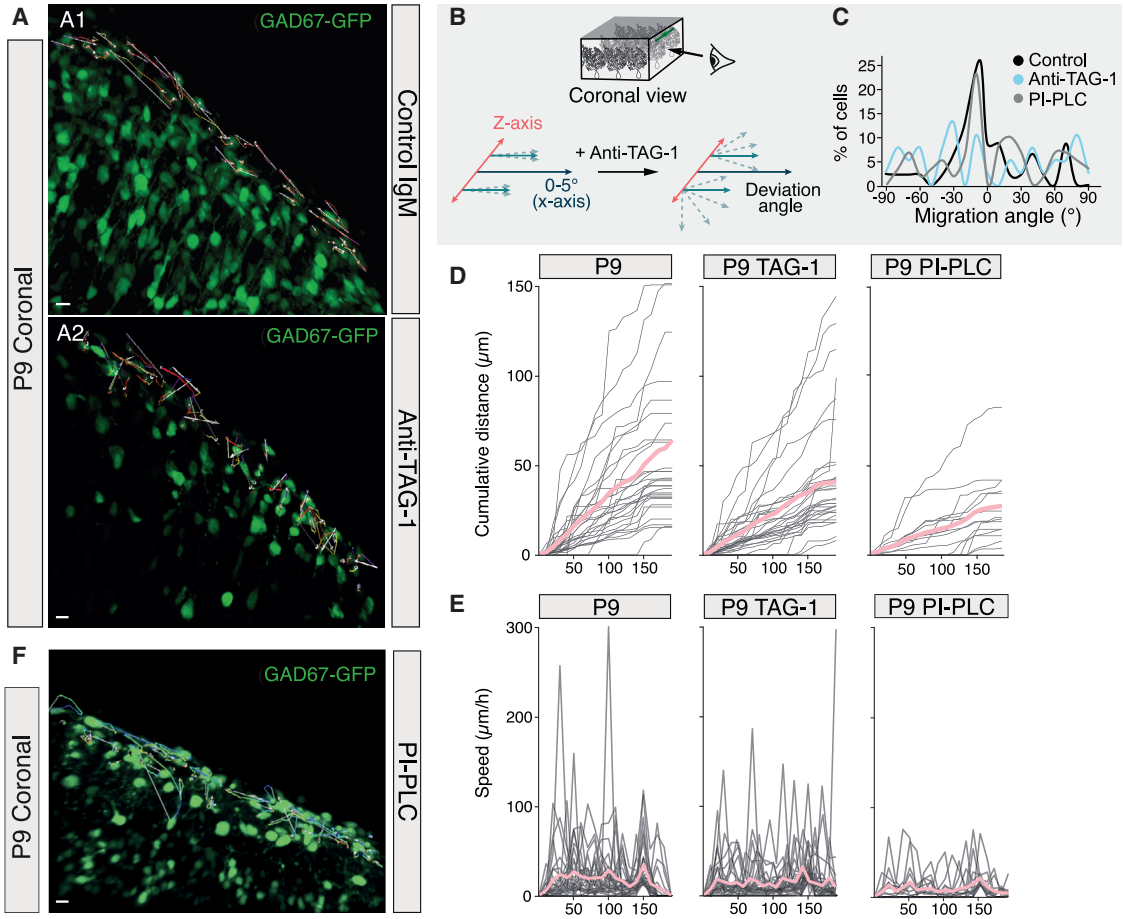

Figure 4. MLGI tangential migration depends on GC TAG-1$^+$ axonal tracts

(A) Migration vectors from live imaging on P9 acute coronal slice from GAD67-GFP BAC transgenic mouse without (A1) or with (A2) the presence of TAG-1 blocking antibody during 1 h before the acquisition. Migratory paths and vectors are represented in pseudo-colors and gray, respectively.

(B) Schema illustrating the effects of TAG-1 blocking antibody application on migration angle values regarding the pial surface.

(C) Diagram showing the distribution of angles of cell trajectories with regard to the pial surface. Under the control condition (black line), a predominant cell population migrates with an angle close to 0°, indicating that their trajectories are parallel to the pial surface defining tangential migration. Application of TAG-1 blocking antibody (light blue line) leads to deviation of MLGI trajectory angle and induces loss of the cell population that migrates with an angle near to 0°. Treatment cleaving GPI-anchored proteins by PI-PLC shows no significant difference compared to control condition. n= 268 (P9 control), 237 (P9 + Anti-TAG-1), and 217 (P9 + PI-PLC).

(D) Cumulative distances achieved by migrating MLGIs at P9 under control, TAG-1 blocking antibody, and PI-PLC conditions in the coronal orientation. The pink curve corresponds to the mean.

(E) Quantification of instantaneous velocities of migrating MLGIs at P9 under control, TAG-1 blocking antibody, and PI-PLC conditions in the coronal orientation. The pink curve corresponds to the mean.

(F) Migration vectors from live imaging on a P9 acute coronal slice after PI-PLC treatment.

Scale bars: 10 μm.

See also Figures S5 and S6 and Video S6.

explore this possibility, we removed TAG-1 from GC neurites. TAG-1 is a GPI-anchored neural cell adhesion molecule that can be cleaved from the cell surface by treatment with phosphatidylinositol-specific phospholipase C (PI-PLC) (Law et al., 2008). After 1 h of treatment with PI-PLC on acute cerebellar slice, TAG-1 expression was no longer detected in the EGL (Figure S5A). Using live imaging after PI-PLC treatment, we observed a significant reduction of both the total distance traveled and speed compared to control (for distance: n = 3 and 4, respectively; 30.1 ± 1.2 versus 61.1 ± 3.4 μm; $p < 0.0001$; for speed: 9.33 ± 2.9 versus 21 ± 3.3 μm/h; $p = 0.0002$) (Figures 4D–4F). In contrast, we did not observe any alteration in MLGI tangential orientation as compared to TAG-1 antibody treatment. This result indicates that TAG-1 protein and/or other GPI-linked molecules are important for the normal migration of MLGIs within iEGL. To further explore the instructive role of TAG-1-positive parallel fiber axons in supporting MLGI migration, we used two experimental *in vitro* models. First, we used a cultured EGL microexplant. In these explants, GCs extend TAG-1-positive fibers away from the core and follow

CellPress
OPEN ACCESS

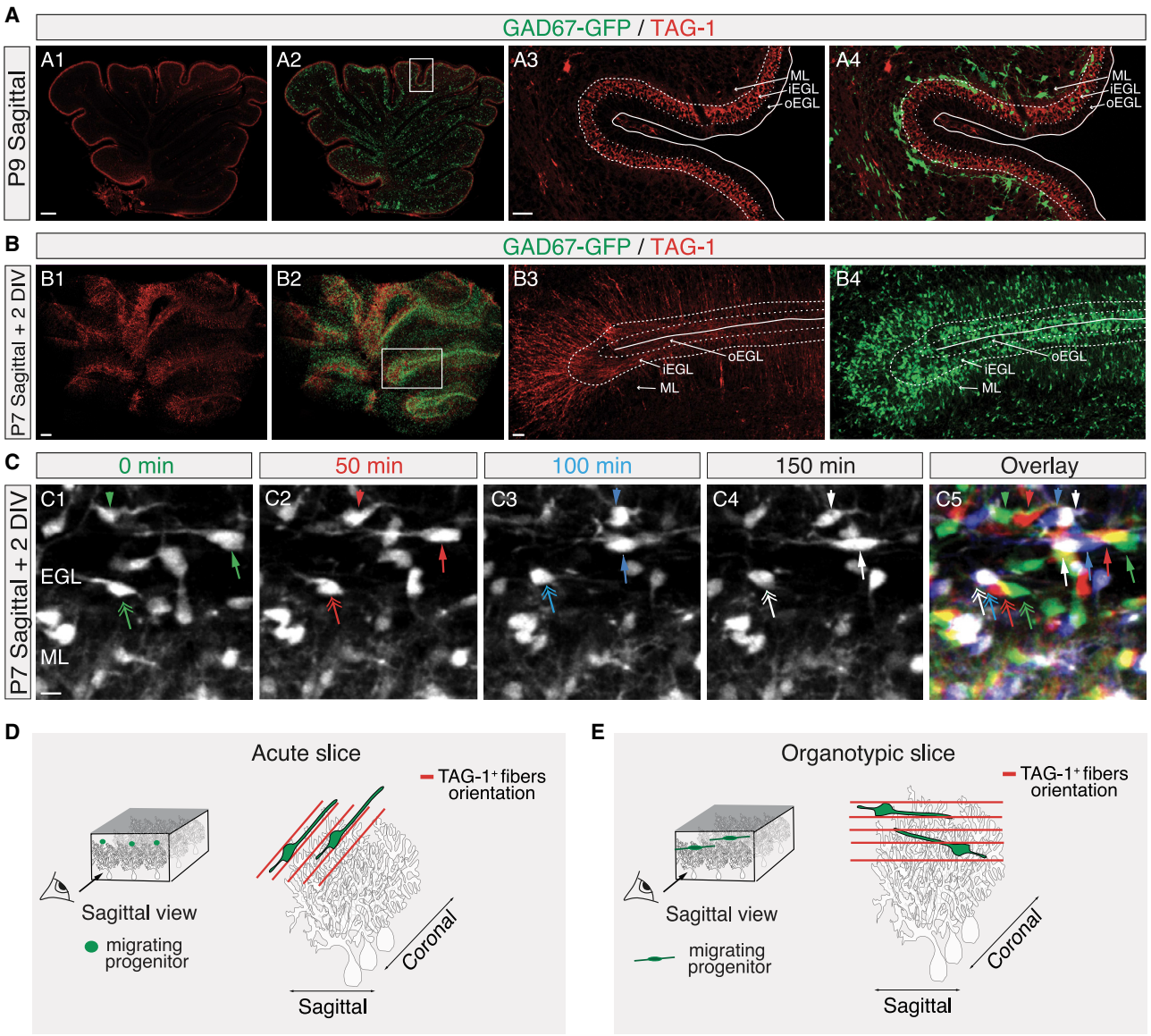

Figure 5. Reorganization of TAG-1 fibers network induces MLGI ectopic tangential migration

(A) TAG-1 (red) immuno-staining on entire sagittal acute slice from GAD67-GFP (green) BAC transgenic mouse at P9 (A1 and A2). TAG-1 is only expressed in the iEGL. Note the presence of GFP-positive cells in the TAG-1 area at high magnification (boxed area) (A3 and A4).

(B) TAG-1 immuno-staining on the entire sagittal organotypic slice from GAD67-GFP BAC transgenic mouse at P7 after 2 days *in vitro* (DIV) (B1 and B2). Expression of TAG-1 is upregulated and not restricted to the iEGL, reflecting the considerable reorganization of premigratory granule fibers (high magnification of boxed area, B3 and B4).

(C) Time-lapse imaging on a sagittal organotypic slice from a GAD67-GFP BAC transgenic mouse at P7 after 2 DIV. On the merged image, a frame corresponding to the start of time lapse (t = 0 min) is pseudo-colored in green, t = 50 min in red, t = 100 min in blue, and t = 150 min in gray. Remodeling of TAG-1-positive fibers induces MLGI tangential migration in the sagittal plane, which is not detectable on sagittal acute slices (Figure S2C).

(D and E) Schematic representation of TAG-1-positive fiber organization on acute sagittal (D) and organotypic slices after 2 DIV (E).

Scale bars: 200 μm in (A1), (A2), (B1), and (B2); 50 μm in (A3), (A4), (B3), and (B4); 10 μm in (C).

See also Video S7.

the same sequence of *in vivo* differentiation (Renaud and Chedotal, 2014). Following GC fiber extension, PAX2-expressing MLGIs emigrated from the explant (Figure S6A). In the presence of the TAG-1 blocking antibody, GCs no longer extended their fibers outside the explants, and MLGIs were unable to emigrate from the core explant, supporting a role for GC TAG-1-positive fibers in MLGI migration (Figures S6B; quantified in Figure S6C). Second, we used a model of sagittal cerebellar organotypic slice culture. In this model, MLGIs display a complex migration pattern, including a phase of tangential

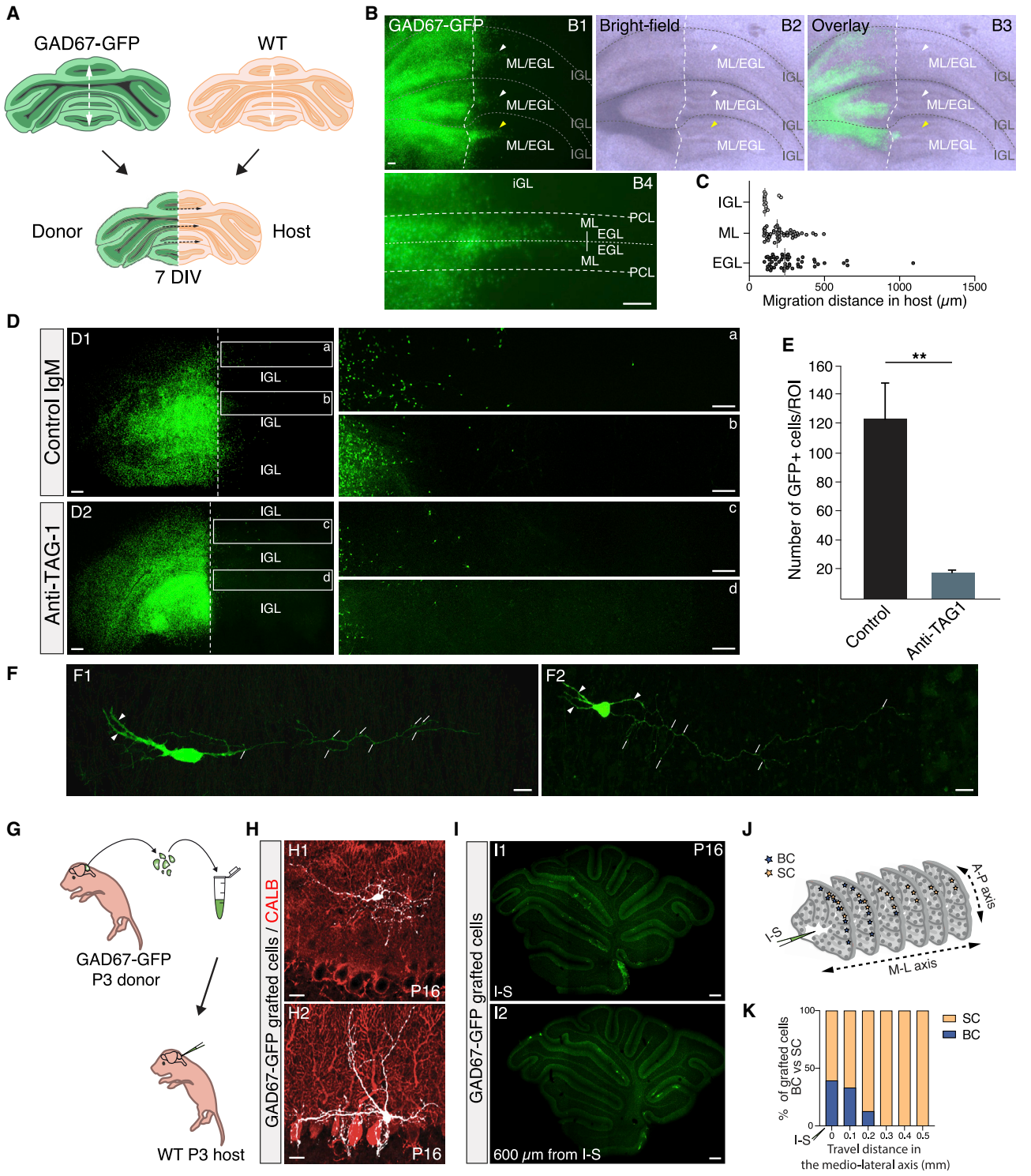

Figure 6. Late-integrating interneurons migrate tangentially in the iEGL and differentiate into the SC subtypes

(A) Schema depicting organo-graft preparation that consists of the association of two coronal slice halves, one from P7 GAD67-GFP BAC transgenic mouse (green) and the other from P7 WT mouse (orange). After 7 DIV, interneurons migrated into the WT side by using several migratory streams (black dotted arrows). (B) Images of organo-graft with the limit between the donor and host sides labeled with a white dotted line (B1–B3). Tangentially GFP$^+$ MLGIs migrating from the donor side to the host side are shown with arrowheads. Cerebellar layers are delineated with gray dotted lines. (B2) is a bright-field image of (B1), and (B3) is a merged image of (B1) and (B2). (B4) is a higher magnification of (B1) pointed by the yellow arrowhead. Note the localization of migrating interneurons in the EGL.

(legend continued on next page)

migration in the ML, which is not observed in acute cerebellar sagittal slices (Cameron et al., 2009). This apparent discrepancy could be explained by a reorganization of TAG-1-positive parallel fiber axons in sagittal organotypic slices. Indeed, the TAG-1-positive area was no longer restricted to the iEGL but was instead ectopically expressed in the oEGL and in the ML (Figures 5A and 5B). In the same preparation, live-imaging experiments revealed ectopic migration of MLGI occurring in both the oEGL and ML (Figure 5C; Video S7). Altogether, our data show that GC axon reorganization in explants and slice cultures is sufficient to induce re-routing of neuron subtypes and further suggest that GC axonal fibers are important to MLGI migration (Figures 5D and 5E).

Tangentially migrating MLGIs are late-integrating cells that differentiate into an SC-like subtype *ex vivo*

During early stages, BC and SC progenitors are morphologically indistinguishable and cannot be discriminated using a genetic marker. To accurately identify MLGI subtypes that underwent tangential migration, individual interneurons need to be tracked until their differentiation. However, no experimental paradigm exists to achieve this challenging task during neuronal circuit development. To address this issue, we set up an experimental paradigm that we called ''organo-grafts'' in which we co-cultured two halves of organotypic P7 cerebellar coronal slices contiguous to one another, as described in Figure 6A. One-half of the organotypic slice is prepared from a GAD67-GFP mouse and the other half from a wild-type (WT) animal. This configuration allows us to identify GFP-positive MLGIs that reach the WT side using tangential migration. After 7 days *in vitro* (DIV), several migratory streams of GFP$^+$ cells were clearly noticeable in the WT host slice (Figure 6B). These streams were located in the EGL (Figures 6B1–6B4; as quantified in Figure 6C) and could reach more than 500 μm from the slice junction. To confirm that cells from the donor side used tangential migration to reach the host side, we inhibited premigratory GC neurite outgrowth by treating organo-grafts with TAG-1 blocking antibody (Figures 6D1 and 6D2). In these experiments, we observed a drastic reduction of the number of GFP$^+$ cells invading the host side compared to the immunoglobulin M (IgM) control condition, showing that the colonization of the host side required tangential migration supported by TAG-1-positive axonal parallel fibers (as quantified in Figure 6E). Moreover, because MLGIs that reached the host side exhibited morphological features similar to those classically observed for SCs (i.e., short dendrites and a beaded axonal arbor) (Figure 6F; Ango et al., 2008), we next grafted GFP-labeled MLGIs *in vivo* to confirm that SCs reached their homing position by using tangential migration. We reasoned that only MLGIs that spread in the mediolateral axis away from the grafting site had used tangential migration.

To this end, we performed a set of grafting experiments allowing us to monitor single-cell integration *in vivo*. Dissociated cells, extracted from GAD67-GFP P3-aged cerebella, were implanted homo-chronically into the cerebellum of P3 WT host mice (Figure 6G). Integration of fluorescent grafted cells was thus analyzed after 13 days in fixed sagittal sections. We looked at the distribution of both SCs (Figure 6H1) and BCs (Figure 6H2) based on their morphological traits. At the injection site, we observed a mixed population of cells composed of both BCs (35%) and SCs (65%) (Figures 6I1, 6J, and 6K). However, in the mediolateral axis, away from the injection site, the percentage of BCs decreased drastically until we observed a 100% SC-like phenotype (Figures 6I2, 6J, and 6K). These data showed that (1) grafted cells could spread along both anteroposterior and mediolateral axes prior to reaching their final location and (2) a fraction of MLGIs migrating over long distances in the mediolateral axis differentiate into SCs.

The SC differentiation program depends on local GC development

To investigate the relative contribution of GCs in the acquisition of SC phenotype, we used *Atoh1*$^{CreER+}$;*Atoh1*$^{Flx/Flx}$ mice to deplete GC precursors from the developing cerebellum (Chang et al., 2019). Because tangential migration occurred in the EGL starting from P7 to P9, *Atoh1*$^{CreER+}$;*Atoh1*$^{Flx/Flx}$ mice were treated with tamoxifen at P1–P3 to drastically reduce the number of GC precursors (Figure S7A). We found that *Atoh1*$^{CreER+}$;*Atoh1*$^{Flx/Flx}$ mice showed a premature reduction of the EGL throughout cerebellar development, which was almost completely depleted at P9 as compared to control *Atoh1*$^{CreER-}$;*Atoh1*$^{Flx/Flx}$ mice (Figures 7A1 and 7B1). In addition, ML from mutant animals appeared reduced compared to that of control mice (Figure S7B). In the absence of

(C) Quantification of the number of interneurons that reach the host side in the IGL, ML, and IGL.
(D) Organo-graft experiments without (D1) or with (D2) TAG-1 blocking antibody. MLGIs from the donor side were detected in the host side (D1) with magnification of boxes a and b and (D2) with magnification of boxes c and d.
(E) Quantification of MLGIs that have undergone tangential migration after 7 DIV under control and TAG-1 blocking antibody conditions. Only those that are 500 μm away from the edge are quantified. Student's t test comparison, **p = 0.005 (n = 6).
(F) Confocal images of GFP$^+$ MLGIs located in the host side after tangential migration. Note some morphological features typical for SCs like short dendrites (white arrowheads) and typical beaded axonal arbor (white arrows).
(G) Schema illustrating transplantation of GFP$^+$ P3 progenitors into WT P3 animals.
(H) Images of grafted SCs (H1) and BCs (H2) 13 days posttransplantation.
(I) Confocal images of the injection site (I1) and 600 μm from the injection site (I2).
(J) Schematic representation of BC (blue stars) and SC (orange stars) dispersion along mediolateral and antero-posterior axes. BCs disperse near the injection site (green pipette) along the antero-posterior axis mainly, whereas SCs are capable of extensive dispersion along the mediolateral axis.
(K) Diagram showing the percentage of grafted BCs (blue) and SCs (orange) integrated along the mediolateral axis. The injection site corresponds to 0 on the horizontal axis. n = 4 with a total of 411 BCs and 1,127 SCs quantified.
Scale bars: 100 μm in (B1)–(B3); 200 μm in (B4), (D1), and (D2); 100 μm in (D1a), (D1b), (D2c), and (D2d); 10 μm in (F); 20 μm in (H); 200 μm in (I). I-S, injection site; A-P, antero-posterior; M-L, mediolateral.

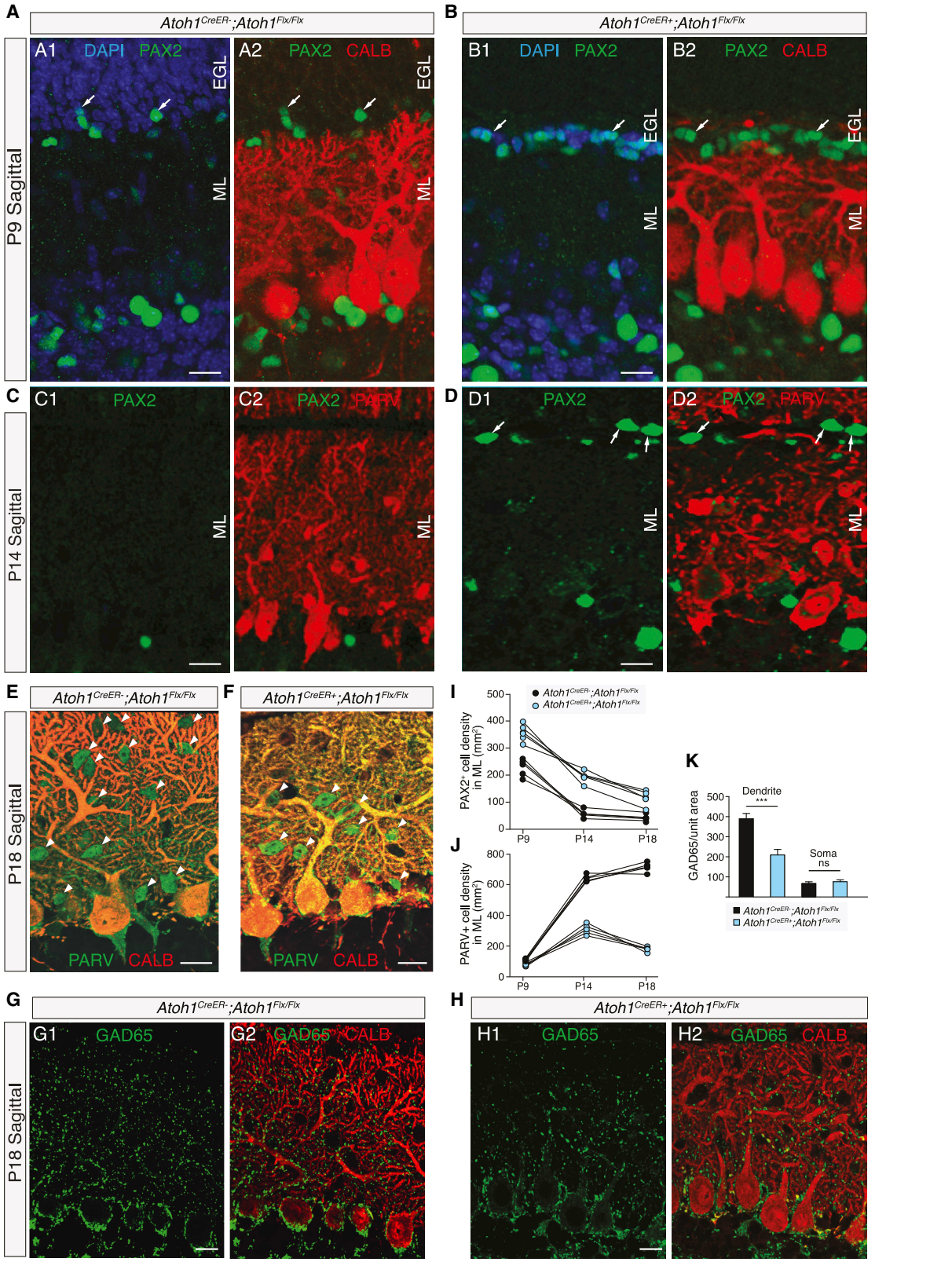

(legend on next page)

EGL, we observed an accumulation of immature PAX2$^+$ cells in *Atoh1*$^{CreER+}$;*Atoh1*$^{Flx/Flx}$ slices above PC dendrites that persisted after P14 and were still detectable after P18 when most PAX2-expressing cells are normally almost absent in control animals (Figures 7C and 7D with quantification in Figure 7I; Figure S7C with quantification in Figure S7D). We next analyzed the maturation of MLGIs by using the mature MLGI marker PARV. The number of PARV$^+$ cells was drastically decreased in *Atoh1*$^{CreER+}$;*Atoh1*$^{Flx/Flx}$ mice compared to control mice in the upper ML, the homing layer for SCs (Figures 7E and 7F; as quantified in Figure 7J). Together, these data show that perturbation of MLGI migration by altering the EGL cellular organization affects MLGI differentiation program. In addition, the deeper part of the ML showed normal PARV expression, whereas the superficial part of the ML, which mostly contains SCs, was completely devoided of PARV$^+$ cell soma in mutants (Figure 7F), suggesting that SC but not BC differentiation is affected.

To demonstrate that SC differentiation and circuit assembly were indeed altered under these conditions, we quantified GABAergic synapses in the ML by using the presynaptic marker GAD65. BCs establish synaptic contacts on both cell soma and AISs of PCs, whereas SCs contact PC dendrites following the fibers of Bergmann glia (Ango et al., 2004; Ango et al., 2008). Thus, it is possible to specifically assess the relative development of both BC and SC presynaptic sites. First, GAD65 density around both soma and AISs of PCs were quantified in mutant *Atoh1*$^{CreER+}$;*Atoh1*$^{Flx/Flx}$ and control mice (Figures 7G and 7H; as quantified in Figure 7K). We observed a comparable distribution and density of GAD65 in both genotypes (n = 4; p = n.s.), suggesting that BC presynaptic contacts were not affected in *Atoh1*$^{CreER+}$;*Atoh1*$^{Flx/Flx}$ mice. Second, we quantified the total number of presynaptic boutons on the dendritic domain of PCs in the ML (Figures 7G and 7H; as quantified in Figure 7K). We observed a nearly 50% reduction of GAD65 labeling in the mutant mice (n = 4; p = 0.0001), showing that SC presynaptic sites were significantly reduced by inducible loss of GCs. Thus, early depletion of premigratory granule cells impaired maturation of SCs and induced a significant decrease in the number of presynaptic GAD65 in the ML. Our data further suggest that local interactions between excitatory and inhibitory progenitors in the cerebellum are critical for interneuron subtype differentiation and proper inhibitory circuit assembly.

DISCUSSION

Cell diversity is the hallmark of CNS function and requires a fine orchestration in space and time of specific neuronal subtype integration into neural circuits. Here, we provide evidence that, although BCs and SCs derive from a common progenitor pool and have an overlapping birth date, their differentiation and integration follow a distinct and specific migration route that impacts their final cell phenotypical traits. We showed that a subset of MLGI progenitors enter the EGL from P7 where they remain immature, as revealed by their continuous expression of PAX2 (Maricich and Herrup, 1999). These cells then undergo an additional step of tangential migration from P9 to P14 before acquiring their final phenotypical traits. This delayed integration, caused by the prolonged migration process, allows the recipient environment to promote a SC-like differentiation, likely through cellular interactions with GC progenitors.

Cellular and molecular mechanisms of MLGI circuit integration

The understanding of MLGI migration and integration into cerebellar neural circuits has remained poorly understood. The seminal work of Goldman and colleagues, using retroviruses, showed that BC and SC precursors are born in the white matter and suggests that they migrate through the PCL to reach the ML (Zhang and Goldman, 1996). Our time-lapse imaging on acute slices revealed that these precursors migrate radially from the GC layer (GCL) to the ML and transiently express PAX2 (Maricich and Herrup, 1999). They display a long leading process through the ML coupled to somal translocation, as reported for radially migrating pyramidal cells (Nadarajah and Parnavelas, 2002). Once they reach their final position, they start their differentiation and express PARV, a marker for mature cerebellar interneurons. The prevailing view is that subsequent precursors enter the ML and position themselves according to a continuous inside-out mode (Yamanaka et al., 2004), where the first interneurons that access the ML will establish close to PC soma and the next ones will populate the upper two-thirds of the ML. However, little is known about the molecular substrates guiding MLGIs from the GCL to their laminar position in the ML. The present study supports a model that allows the subsequent waves of migrating interneurons to enter the ML in an inside-out manner. Although early-born MLGIs enter the ML outside the TAG-1 region, later ones use the TAG-1-positive environment as a substrate for their extended tangential migration. The first migration waves, localized below the TAG-1-positive area, occur between P3 and P7 and correspond to the differentiation window of

Figure 7. Depletion of granule cell precursors affects late-born MLGI maturation

(A–D) Confocal images of sagittal cerebellar slices from P9 (A and B) and P14 (C and D) control and *Atoh1*$^{CreER+}$;*Atoh1*$^{Flx/Flx}$ mice double stained with PAX2 (green), CALB (A2 and B2), or PARV (C2 and D2) (red). PAX2+ immature MLGIs located in EGL are marked with white arrows.

(E and F) Immunolabeled P18 sagittal *Atoh1*$^{CreER+}$;*Atoh1*$^{Flx/Flx}$ and control mice sections with CALB (red) and PARV (green). Mature MLGIs are marked with white arrowheads.

(G and H) Immunolabeled P18 sagittal *Atoh1*$^{CreER+}$;*Atoh1*$^{Flx/Flx}$ and control mice sections with CALB (red) and GAD65 (green).

(I) Quantification of PAX2 cell density in ML at P9, P14, and P18 in *Atoh1*$^{CreER+}$;*Atoh1*$^{Flx/Flx}$ and WT animals.

(J) Quantification of PARV-positive cells in ML at P9, P14, and P18 in *Atoh1*$^{CreER+}$;*Atoh1*$^{Flx/Flx}$ and WT mice.

(K) Quantification of GAD65 density in the entire ML at the level of Purkinje dendritic tree and around soma and AIS of Purkinje cells.

Scale bars: 20 μm. PARV, parvalbumin; AIS, axonal initial segment. Unpaired t test comparison for PAX2 at P9, *p = 0.001 (n = 5); at P14, **p = 0.0001 (n = 4); and at P18, **p = 0.005 (n = 4); and comparison for PARV at P9, not significant (n.s.) (n = 5); at P14, ***p = 0.00001 (n = 4); and at P18, ***p = 0.00001 (n = 4).

See also Figure S7.

BCs that are kept outside the EGL. This population might be sensitive to netrin repulsion (Guijarro et al., 2006). During the second and subsequent waves, MLGIs enter the TAG-1 positive area, corresponding to the lower part of the EGL, just above the ML. At this level, the neural cell adhesion molecule TAG-1 is expressed along the axonal processes of the GC precursors. As the EGL develops, GC precursors will progressively cease to express TAG-1 and migrate radially to form the internal granule cell layer (IGL). At the same time, GC precursors located just above the previous ones in the EGL will start to express TAG-1, thus creating a new scaffold for the integration of newly arrived MLGIs. It is worth noting that the outside-in developmental pattern of the EGL supports the establishment of the inside-out mode of MLGI integration.

The identification of the TAG-1-positive axonal parallel fibers as a substrate for tangentially migrating interneurons was also identified in the cortex for interneurons migrating along the corticofugal axons (Denaxa et al., 2001; McManus et al., 2004; Morante-Oria et al., 2003). Intriguingly, the birth date of GABAergic interneurons restrains their ability to use TAG-1-positive axons as a scaffold for migration, as also shown in the present study (McManus et al., 2004), suggesting that temporal differences have an impact on substrate specificities. Thus, it is tempting to speculate that, in both cerebral and cerebellar cortices, specific migration substrates that control distinct migration routes might also contribute to the cell-type diversity program by exposing neuronal precursors to specific environmental cues.

Specific migration routes for MLGI integration in the cerebellar circuit

In the cerebellum, BCs and SCs are thought to belong to the same cell type. The inside-out sequence of MLGI integration was suggested to provide a common mechanism to link their phenotypes and laminar position in cerebellar ML to their birth date. However, interneurons that are born at the same time and share the same laminar localization display different phenotypes, questioning how the same local environment might affect their identity. We were able to show that the timing of integration, which depends on the migration route used to reach the final location, is critical for proper neuronal integration and normal neural circuit formation. Indeed, we observed two distinct migration patterns for neuronal precursors that reach the ML. One population of MLGIs, the BCs, starts to differentiate immediately after reaching the ML, as identified by the loss of PAX2 expression and the subsequent expression of the mature neuronal marker PARV. During the same time window, a fraction of cells enters the EGL and performs an additional step of tangential migration and, therefore, delays the onset of its differentiation. We hypothesize that this delay in differentiation onset contributes to a change in environmental cues and, therefore, participates in the cell diversity program. Indeed, depletion of the EGL in the *Atoh1*$^{CreER+}$;*Atoh1*$^{Flx/Flx}$ mice altered the differentiation program of the late-born SC subtypes that remained immature and failed to develop proper synaptic connectivity in contrast to BCs. Although depletion of GCs at the earliest time point might equally affect BC and SC differentiation, we think that this is unlikely for the following reasons. First, temporal fate mapping of cerebellar interneurons by using the *Ascl1*^{CreER} mice revealed that tamoxifen injection from P1 to P7 mainly labels SCs, indicating that the majority of BCs are already specified before P1 (Sudarov et al., 2011). Second, although a fraction of BCs is already differentiated in the ML before P5, we were unable to detect MLGIs in the EGL, suggesting that the differentiation of BCs does not require interaction with TAG-1-positive GCs. Third, in *NeuroD2* knockout mice, BCs remained PAX2 immunopositive, failed to express PARV, and did not innervate PC AIS; whereas normal SC dendritic innervation was preserved (Pieper et al., 2019). Thus, BC and SC differentiation programs appear to be regulated by distinct mechanisms. Altogether, these results add arguments in favor of the distinctive neuron subtype classification of BCs versus SCs and report their divergent migration, integration, and differentiation into the ML.

Recent data in the cerebellum indicate that synaptic activity from GCs regulates GABAergic interneuron final positioning in the ML (Park et al., 2019). Increasing evidence suggests that subtle changes in migration patterns might result from genomic mutations associated with circuit dysfunction. In the future, it will be important to examine how defects in migration route impact the neuronal differentiation and cell identity program during neural circuit development.

STAR★METHODS

Detailed methods are provided in the online version of this paper and include the following:

- KEY RESOURCES TABLE
- RESOURCE AVAILABILITY
  - Lead contact
  - Materials availability
  - Data and code availability
- EXPERIMENTAL MODEL AND SUBJECT DETAILS
  - Mouse lines
  - Animal statement
- METHOD DETAILS
  - Immunohistochemistry
  - Two-photon imaging on acute slices
  - Organotypic slice culture
  - Transplantation experiments
  - Microexplant preparation
- QUANTIFICATION AND STATISTICAL ANALYSIS
  - Image analysis
  - Movie analysis
  - Statistical analysis

SUPPLEMENTAL INFORMATION

Supplemental information can be found online at https://doi.org/10.1016/j.celrep.2021.108904.

ACKNOWLEDGMENTS

This work was supported by ANR-14-CE12-0015-03 and ERA-Net NEURON/DECODE (18-NEUR-0004) to F.A. D.J.H. was supported by

MRC (MR/N00275X/1 and MR/S025618/1) and Diabetes UK (17/0005681) project grants. This project has received funding from the European Research Council (ERC) under the European Union's Horizon 2020 research and innovation program (starting grant 715884 to D.J.H.). P.M. was supported by the Agence Nationale de la Recherche (ANR-15-CE14-0012-01 and ANR-18-CE14-0017-01) and France-Bioimaging (INBS10-GaL/AR-11/12). C.C. was supported by a fellowship from the French Ministry of Research and Education. We thank Pierre Fontanaud for his help in initial video tracking analysis and the iExplore and RIO-Imaging Platforms of the IGF for their support. We also thank IGF direction and J.P. Pin for their support of this project.

AUTHOR CONTRIBUTIONS

F.A. managed the study; C.C., I.B., and F.A. designed the experiments. A.F. and O.A. performed the *Atoh1* KD experiments. A.J.F. provided TAG-1 mutant brains. C.C. performed live-imaging experiments with the help of D.J.H. C.C. and I.B. performed immunohistochemistry and micro-explant and organograft experiments with the help of C.J.-T. C.C., I.B., and F.A. analyzed the data. C.C. and F.A. wrote the manuscript with the help of P.M., D.J.H., and C.S.

DECLARATION OF INTERESTS

The authors declare no competing interests.

Received: March 26, 2020
Revised: December 19, 2020
Accepted: March 3, 2021
Published: March 30, 2021

REFERENCES

Ango, F., di Cristo, G., Higashiyama, H., Bennett, V., Wu, P., and Huang, Z.J. (2004). Ankyrin-based subcellular gradient of neurofascin, an immunoglobulin family protein, directs GABAergic innervation at purkinje axon initial segment. Cell *119*, 257–272.

Ango, F., Wu, C., Van der Want, J.J., Wu, P., Schachner, M., and Huang, Z.J. (2008). Bergmann glia and the recognition molecule CHL1 organize GABAergic axons and direct innervation of Purkinje cell dendrites. PLoS Biol. *6*, e103.

Ascoli, G.A., Alonso-Nanclares, L., Anderson, S.A., Barrionuevo, G., Benavides-Piccione, R., Burkhalter, A., Buzsáki, G., Cauli, B., Defelipe, J., Fairén, A., et al.; Petilla Interneuron Nomenclature Group (2008). Petilla terminology: nomenclature of features of GABAergic interneurons of the cerebral cortex. Nat. Rev. Neurosci. *9*, 557–568.

Blot, A., and Barbour, B. (2014). Ultra-rapid axon-axon ephaptic inhibition of cerebellar Purkinje cells by the pinceau. Nat. Neurosci. *17*, 289–295.

Cameron, D.B., Kasai, K., Jiang, Y., Hu, T., Saeki, Y., and Komuro, H. (2009). Four distinct phases of basket/stellate cell migration after entering their final destination (the molecular layer) in the developing cerebellum. Dev. Biol. *332*, 309–324.

Carter, R.A., Bihannic, L., Rosencrance, C., Hadley, J.L., Tong, Y., Phoenix, T.N., Natarajan, S., Easton, J., Northcott, P.A., and Gawad, C. (2018). A Single-Cell Transcriptional Atlas of the Developing Murine Cerebellum. Curr. Biol. *28*, 2910–2920.e2.

Chang, C.H., Zanini, M., Shirvani, H., Cheng, J.S., Yu, H., Feng, C.H., Mercier, A.L., Hung, S.Y., Forget, A., Wang, C.H., et al. (2019). Atoh1 Controls Primary Cilia Formation to Allow for SHH-Triggered Granule Neuron Progenitor Proliferation. Dev. Cell *48*, 184–199.e5.

DeFelipe, J., López-Cruz, P.L., Benavides-Piccione, R., Bielza, C., Larrañaga, P., Anderson, S., Burkhalter, A., Cauli, B., Fairén, A., Feldmeyer, D., et al. (2013). New insights into the classification and nomenclature of cortical GABAergic interneurons. Nat. Rev. Neurosci. *14*, 202–216.

Denaxa, M., Chan, C.H., Schachner, M., Parnavelas, J.G., and Karagogeos, D. (2001). The adhesion molecule TAG-1 mediates the migration of cortical interneurons from the ganglionic eminence along the corticofugal fiber system. Development *128*, 4635–4644.

Furley, A.J., Morton, S.B., Manalo, D., Karagogeos, D., Dodd, J., and Jessell, T.M. (1990). The axonal glycoprotein TAG-1 is an immunoglobulin superfamily member with neurite outgrowth-promoting activity. Cell *61*, 157–170.

Guijarro, P., Simó, S., Pascual, M., Abasolo, I., Del Río, J.A., and Soriano, E. (2006). Netrin1 exerts a chemorepulsive effect on migrating cerebellar interneurons in a Dcc-independent way. Mol. Cell. Neurosci. *33*, 389–400.

Huang, Z.J., and Paul, A. (2019). The diversity of GABAergic neurons and neural communication elements. Nat. Rev. Neurosci. *20*, 563–572.

Kepecs, A., and Fishell, G. (2014). Interneuron cell types are fit to function. Nature *505*, 318–326.

Kole, M.J., Qian, J., Waase, M.P., Klassen, T.L., Chen, T.T., Augustine, G.J., and Noebels, J.L. (2015). Selective Loss of Presynaptic Potassium Channel Clusters at the Cerebellar Basket Cell Terminal Pinceau in Adam11 Mutants Reveals Their Role in Ephaptic Control of Purkinje Cell Firing. J. Neurosci. *35*, 11433–11444.

Law, C.O., Kirby, R.J., Aghamohammadzadeh, S., and Furley, A.J. (2008). The neural adhesion molecule TAG-1 modulates responses of sensory axons to diffusible guidance signals. Development *135*, 2361–2371.

Lim, L., Mi, D., Llorca, A., and Marín, O. (2018). Development and Functional Diversification of Cortical Interneurons. Neuron *100*, 294–313.

Machold, R., and Fishell, G. (2005). Math1 is expressed in temporally discrete pools of cerebellar rhombic-lip neural progenitors. Neuron *48*, 17–24.

Maricich, S.M., and Herrup, K. (1999). Pax-2 expression defines a subset of GABAergic interneurons and their precursors in the developing murine cerebellum. J. Neurobiol. *41*, 281–294.

Marín, O. (2012). Interneuron dysfunction in psychiatric disorders. Nat. Rev. Neurosci. *13*, 107–120.

McManus, M.F., Nasrallah, I.M., Gopal, P.P., Baek, W.S., and Golden, J.A. (2004). Axon mediated interneuron migration. J. Neuropathol. Exp. Neurol. *63*, 932–941.

Morante-Oria, J., Carleton, A., Ortino, B., Kremer, E.J., Fairén, A., and Lledo, P.M. (2003). Subpallial origin of a population of projecting pioneer neurons during corticogenesis. Proc. Natl. Acad. Sci. USA *100*, 12468–12473.

Nadarajah, B., and Parnavelas, J.G. (2002). Modes of neuronal migration in the developing cerebral cortex. Nat. Rev. Neurosci. *3*, 423–432.

Park, H., Kim, T., Kim, J., Yamamoto, Y., and Tanaka-Yamamoto, K. (2019). Inputs from Sequentially Developed Parallel Fibers Are Required for Cerebellar Organization. Cell Rep. *28*, 2939–2954.e5.

Pieper, A., Rudolph, S., Wieser, G.L., Götze, T., Mießner, H., Yonemasu, T., Yan, K., Tzvetanova, I., Castillo, B.D., Bode, U., et al. (2019). NeuroD2 controls inhibitory circuit formation in the molecular layer of the cerebellum. Sci. Rep. *9*, 1448.

Rakic, P. (1973). Kinetics of proliferation and latency between final cell division and onset of differentiation of cerebellar stellate and basket neurons. J. Comp. Neurol. *147*, 523–546.

Renaud, J., and Chedotal, A. (2014). Time-lapse analysis of tangential migration in Sema6A and PlexinA2 knockouts. Mol. Cell. Neurosci. *63*, 49–59.

Shroyer, N.F., Helmrath, M.A., Wang, V.Y., Antalffy, B., Henning, S.J., and Zoghbi, H.Y. (2007). Intestine-specific ablation of mouse atonal homolog 1 (Math1) reveals a role in cellular homeostasis. Gastroenterology *132*, 2478–2488.

Simat, M., Ambrosetti, L., Lardi-Studler, B., and Fritschy, J.M. (2007). GABAergic synaptogenesis marks the onset of differentiation of basket

and stellate cells in mouse cerebellum. Eur. J. Neurosci. *26*, 2239–2256.

Stottmann, R.W., and Rivas, R.J. (1998). Distribution of TAG-1 and synaptophysin in the developing cerebellar cortex: relationship to Purkinje cell dendritic development. J. Comp. Neurol. *395*, 121–135.

Sudarov, A., Turnbull, R.K., Kim, E.J., Lebel-Potter, M., Guillemot, F., and Joyner, A.L. (2011). Ascl1 genetics reveals insights into cerebellum local circuit assembly. J. Neurosci. *31*, 11055–11069.

Telley, L., Cadilhac, C., Cioni, J.-M., Saywell, V., Jahannault-Talignani, C., Huettl, R.E., Sarrailh-Faivre, C., Dayer, A., Huber, A.B., and Ango, F. (2016). Dual Function of NRP1 in Axon Guidance and Subcellular Target Recognition in Cerebellum. Neuron *91*, 1276–1291.

Wamsley, B., and Fishell, G. (2017). Genetic and activity-dependent mechanisms underlying interneuron diversity. Nat. Rev. Neurosci. *18*, 299–309.

Wang, W., Karagogeos, D., and Kilpatrick, D.L. (2011). The effects of Tag-1 on the maturation of mouse cerebellar granule neurons. Cell. Mol. Neurobiol. *31*, 351–356.

Yamanaka, H., Yanagawa, Y., and Obata, K. (2004). Development of stellate and basket cells and their apoptosis in mouse cerebellar cortex. Neurosci. Res. *50*, 13–22.

Zhang, L., and Goldman, J.E. (1996). Generation of cerebellar interneurons from dividing progenitors in white matter. Neuron *16*, 47–54.

STAR★METHODS

KEY RESOURCES TABLE

REAGENT or RESOURCE	SOURCE	IDENTIFIER
Antibodies		
Mouse monoclonal anti-TAG-1	DSHB	Cat#4D7/TAG1; RRID: AB_531775
Chicken polyclonal anti-Beta III Tubulin	Merck Millipore	Cat#AB9354; RRID: AB_570918
Mouse monoclonal anti-Parvalbumin	Merck Millipore	Cat#MAB1572; RRID: AB_2174013
Rabbit polyclonal anti-Parvalbumin	Swant	Cat#PV-28; RRID: AB_2315235
Mouse monoclonal anti-Calbindin	Swant	Cat#300; RRID: AB_10000347
Rabbit polyclonal anti-Calbindin	Swant	Cat#CB38; RRID: AB_10000340
Rabbit polyclonal anti-PAX2	Thermo Fisher Scientific	Cat#71-6000; RRID: AB_2533990
Mouse monoclonal Anti-Drosophila tracheal system (Control IgM)	DSHB	Cat#2A12; RRID:AB_528492
Chemicals, peptides, and recombinant proteins		
CyTRAK Orange	Abcam	Cat#ab109203
16% Formaldehyde (w/v), Methanol-free	Thermo Scientific	Cat#28908
Basal Medium Eagle (BME)	Thermo Scientific	Cat#21010046
Neurobasal medium	Thermo Scientific	Cat#21103049
B27 Supplement	Thermo Scientific	Cat#17504044
Normal Horse serum	Vector Laboratories	Cat#S2000
Sucrose	Sigma-Aldrich	Cat#S0389
Hanks' Balanced Salt solution (HBSS)	Sigma-Aldrich	Cat#H8264
Penicillin Streptomycin solution	Sigma-Aldrich	Cat#P4333
GlutaMAX Supplement	Thermo Scientific	Cat#35050038
Triton X-100	Sigma-Aldrich	Cat#T8787
Vectashield hard-set with DAPI	Vector Laboratories	Cat#H-1500; RRID: AB_2336788
Phospholipase C, Phosphatidylinositol-specific from *Bacillus cereus*	Sigma-Aldrich	Cat#P8804
Tissue-Tek O.C.T. Compound	Sakura	Cat#4583
Tamoxifen	Sigma-Aldrich	Cat#T5648
Poly-L-Lysine	Sigma-Aldrich	Cat#P1274
Laminin	Sigma-Aldrich	Cat#L2020
BSA	Sigma-Aldrich	Cat#05470
L-Thyroxine	Sigma-Aldrich	Cat#T2376
Transferrin	Sigma-Aldrich	Cat#T8158
Insulin	Sigma-Aldrich	Cat#I6634
Aprotinin	Sigma-Aldrich	Cat#A1153
Experimental models: organisms/strains		
Mouse: CB6-Tg(Gad1-EGFP)G42Zjh/J (G42 line)	The Jackson Laboratory	Cat#JAX:007677; RRID: IMSR_JAX:007677
Mouse: Tg(Atoh1-cre/Esr1*)14Fsh/J	The Jackson Laboratory	Cat#JAX:007684; RRID: IMSR_JAX:007684
Mouse: B6.129S7-*Atoh1*^{tm3Hzo}/J	The Jackson Laboratory	Cat#JAX:008681; RRID: IMSR_JAX:008681
Software and algorithms		
Fiji	NIH	RRID: SCR_002285, https://fiji.sc/
ZEN Digital Imaging for Light Microscopy	Zeiss	RRID: SCR_013672

(*Continued on next page*)

Continued

REAGENT or RESOURCE	SOURCE	IDENTIFIER
GraphPad Prism 8	GraphPad software	RRID: SCR_002798
R	R Core Team	https://www.r-project.org
Imaris	Bitplane	RRID:SCR_007370
Adobe Illustrator 2020	Adobe Systems	https://www.adobe.com/products/illustrator.html; RRID: SCR_010279

RESOURCE AVAILABILITY

Lead contact

Further information and requests for resources and reagents should be directed to and will be fulfilled by the lead contact, Fabrice Ango (fabrice.ango@inserm.fr).

Materials availability

This study did not generate new unique reagents.

Data and code availability

This study did not generate new dataset and no custom code was used in this study.

EXPERIMENTAL MODEL AND SUBJECT DETAILS

Mouse lines

Swiss wild-type mice used for transplantation and organo-graft experiments were obtained from Janvier Labs. GAD67-GFP BAC transgenic mice have previously been described (Ango et al., 2004). *Atoh1*^{CreER} (referred to as *Tg(Atoh1- cre/Esr1***)14Fsh*) (Machold and Fishell, 2005) and *Atoh*$^{Flx/Flx}$ (referred to as *Atoh1*^{tm3Hzo}) (Shroyer et al., 2007) were all obtained from Jackson Laboratory. To achieve the conditional knockout of *Atoh1* in GNPs, *Atoh1*$^{CreER+}$*;Atoh1*$^{Flx/Flx}$ mice were intraperitoneally injected with tamoxifen at P3. Housing conditions consisted of cages containing a maximum of 6 adult mice. Breeding cages contained 1 male and up to 2 females. For all the experiments, both males and females were used. We used P3, P5, P7, P9, P12, P14 and P18 animals for experiments.

Animal statement

The experimental plan was designed according to the European Communities Council Directive and the French law for care and use of experimental animals. We followed the European and national regulations for the care and use of animals in order to protect vertebrate animals for experimental and other scientific purposes (Directive 86/609). The project ''Atoh1/Math1 regulation and function during cerebellar normal development and medulloblastoma'' obtained the ethical approval (#2011-0012) from the reporting ethical committee IDF Paris-Comité 1. Use of animals was also approved by the Institutional Animal Care and Use Committee (IACUC) of National Yang-Ming University (1030503, 1040625).

METHOD DETAILS

Immunohistochemistry

For tissue preparation, animals were euthanized by intraperitoneal injection of Pentobarbital (50 mg/kg) and perfused intracardiacally with cold artificial cerebrospinal fluid (aCSF) (NaCl, 126 mM; KCl, 3 mM; NaH_2PO_4, 1.25 mM; $NaHCO_3$, 20 mM; $MgSO_4$, 2 mM; $CaCl_2$, 2 mM and D-glucose, 20 mM, pH 7.4). Cerebella were dissected and fixed overnight (O/N) in cold paraformaldehyde 4% before slicing at 60 μm-thick and stored at 4°C in phosphate buffer saline. For certain immunostaining protocols, brains were cryoprotected with 20% and 30% sucrose in PBS successively and then frozen in O.C.T compound. Brains were finally cut sagittally or coronally on a sliding cryotome at 50 μm and sections were kept in a cryoprotective solution at −20°C. For immunostaining, slices were treated with blocking reagent (5% normal horse serum, 0.2% Triton X-100 in PBS) for 3 hours at room temperature before incubating with the following primary antibodies O/N at 4°C: mouse anti-Parvalbumin (1/1000, Chemicon), rabbit anti-Parvalbumin (1/500, Swant), mouse anti-Calbindin (1/500, Swant), rabbit anti-Calbindin (1/1000, Swant), rabbit anti-PAX2 (1/100, Invitrogen), mouse anti-TAG- 1 (1/125, DSHB), chicken anti-TUJ1 (1/500, Millipore). Secondary goat Alexa 488, −546, −633 (Invitrogen) or donkey

NL-493, −557, −637 (R&D) raised against the appropriate species were used at a dilution of 1/1000 and sections were mounted in Vectashield hard-set with DAPI (Vector Laboratories).

Two-photon imaging on acute slices

GAD67-GFP BAC transgenic mice were decapitated and brains were quickly transferred into ice-cold aCSF (NaCl, 126 mM; KCl, 3 mM; NaH2PO4, 1.25 mM; NaHCO3, 20 mM; MgSO4, 2 mM; CaCl2, 2 mM and D-glucose, 20 mM, pH 7.4). After removing the cerebellum from the skull, cerebellar coronal or sagittal slices 300 μm-thick were cut with a vibratome, allowed to recover for one hour in oxygenated aCSF at 34°C and immersed in an environmentally-controlled recording chamber at 37°C, 5% O2 / 95% CO2. For CyTRAK experiments, Orange dye application (1/500, Abcam) was performed for 15 minutes just before the acquisition. For blocking antibody and PI-PLC experiments, TAG-1 (250 μg/ml, DSHB), control IgM (250 μg/ml, DSHB) and PI-PLC (0.5 U/ml, Sigma) were incubated for one hour at 37°C prior to imaging. Images (300 μm x 300 μm) were acquired with a two-photon microscope (TriM Scope, LaVision Biotec) equipped with a water immersion X20, 0,95NA objective (Olympus). The Ti-Sapphire laser (Chameleon, Coherent) was tuned to the optimal excitation wavelength for GFP (900 nm), with emitted signals detected at 910 nm using a PMT. Excitation for CyTRAK Orange was delivered at 970 nm, with emitted signals detected at 980 nm. Movies were made from 3D stacks (z = 200 μm) acquired sequentially every 10 min using a step size of 2 μm. At least 5 acquisition sessions per condition were analyzed and each acquisition was made from distinct animals (n = 5).

Organotypic slice culture

GAD67-GFP BAC transgenic and WT pups were rapidly decapitated and dissected in cold HBSS. Cerebella were removed from the skull and cut using a tissue-chopper into 350 μm- thick sagittal or coronal slices. Immediately, slices were transferred to the membrane of culture inserts (Millicell, Millipore) with prewarmed medium containing a mix of BME/HBSS (Sigma- Aldrich) supplemented with glutamine, 5% horse serum and 1% pen/strep (Sigma-Aldrich) for incubation (37°C, 5% CO2). For blocking antibody experiments, organotypic cerebellar slices were incubated with the TAG-1 antibody (250 μg/ml, DSHB) or control IgM (250 μg/ml, DSHB) for 8DIV, renewing the medium every two days. For organo-graft experiments, two halves of organotypic cerebellar coronal slices (one from a WT animal and one from a GAD67- GFP BAC transgenic one) contiguous one to the other were cultivated.

Transplantation experiments

For cell preparation, P3 GAD67-GFP BAC transgenic pups were rapidly decapitated and dissected in cold HBSS (Sigma-Aldrich). Cerebella were extracted from the skull before gently removing meninges and choroid plexus. Cerebella were then cut using a tissue-chopper into 300 μm-thick sagittal slices collected in neurobasal medium (NB, Thermo Scientific). Cerebellar cells were mechanically dissociated using three sterile glass pipettes with decreasing diameter. Obtained suspensions were then centrifuged and resuspended at a final concentration of 1 X 10^5 cells/μl in NB containing B27 supplement (2%, Thermo Scientific) and GlutaMax (1%, Thermo Scientific). For the transplantation process, P3 pups were cryo-anesthetized in melting ice, a midline incision of the scalp was performed, and muscles were gently removed from skull bone with a tweezer. After setting stereotaxic coordinates, a small hole in the skull was done using a needle and 2 μl of the final suspension was injected in the vermis of the cerebellar cortex thanks to a glass micropipette. Finally, the wound was sutured and pups were put back with the mother. The recipient animals were killed 13 days after transplantation.

Microexplant preparation

P3 WT pups were rapidly decapitated and dissected in cold HBSS (Sigma-Aldrich). Cerebella were extracted from the skull before gently removing meninges and choroid plexus. Cerebellums were then cut using a tissue-chopper into 300 μm-thick sagittal slices. Squared pieces (300 × 300 μm) were micro-dissected and plated on previously coated coverslips with poly-L-lysine (200 μg/ml, Sigma-Aldrich) and laminin (20 μg/ml, Sigma-Aldrich). To culture cerebellar microexplants, a complemented BME medium (Thermo Scientific) was freshly prepared containing BSA (1 mg/ml, Sigma-Aldrich), L-Thyroxine (1 nM, Sigma-Aldrich), Transferrin (100 μg/ml, Sigma-Aldrich), Insulin (10 μg/ml, Sigma-Aldrich), Aprotinin (1 μg/ml, Sigma-Aldrich), pen/strep (1%, Sigma-Aldrich) and GlutaMax (1%, Thermo Scientific). After 1 DIV in the incubator (37°C, 5% CO2), microexplants were finally fixed with paraformaldehyde 4% for 10 minutes, permeabilized with 1% Triton for 5 minutes, immunostained with PAX2 (Rabbit, 1/100), TUJ1 (Chicken, 1/500) primary antibodies and counterstained with DAPI. For TAG-1 condition, anti-TAG-1 blocking antibody (250 μg/ml, DSHB) was added to the culture medium 4 hours after plating.

QUANTIFICATION AND STATISTICAL ANALYSIS

Image analysis

Immunofluorescence experiments were imaged at high magnification by confocal laser- scanning microscopy (Zeiss LSM 780). Images were acquired either with 40X or 20X lenses (NA 1.3). For display, images were superimposed and processed with the image analysis softwares Imaris (Bitplane) and ImageJ (NIH). In order to define the boundary between ML and EGL after live imaging sessions, DAPI staining was performed on fixed slices and images from the area of interest were acquired. Speed and traveled distances from live-imaging experiments were analyzed and plotted using R and GraphPadPrism8 (GraphPad). Deviation angles from the mediolateral axis shown in Figure 4C were defined by calculating the inverse tangent of (Δz/Δx) ratio for each cell. For organo-grafts analysis,

only GFP-positive cells from the donor side that have migrated more than 500 μm in the host side were counted. To determine injection site for grafting experiments, stereotaxic coordinates were used in addition to scar that was still visible at the level of the dura. Another important indicator is the presence of few GFP positive cells in the IGL around the injection site and as you move from the injection site, the number of cells in the IGL is decreasing. BC and SC identities were defined according to morphology, location into the ML and axonal targeting. For cerebellar microexplant analysis, the length of TUJ1+ fibers was measured from the explant border. For the analysis of GFP and TAG-1 signal apposition, we used the "plot profile" function from ImageJ software (NIH) to measure the pixel intensity of GFP and TAG-1 along a straight line crossing multiple GFP positive neurites in the EGL. After splitting the two channels, the line was added as a ROI and used to analyze TAG-1 signal intensity. Pixel intensity along this line was measured individually in both channels. Numbers of GFP peaks identified with an overlap with a peak of TAG-1 were collected and data were analyzed using GraphPadPrism8.

Movie analysis

After translational and rotational drift correction, 2-photon acquisitions were analyzed using the 3D-tracking tool from Imaris software (Bitplane) and quantitative data were exported for further speed, traveled distance and deviation angle measurements analyses. Movies were finally annotated using Manual Tracking ImageJ plugin (https://imagej.net/Manual_Tracking).

Statistical analysis

Sample sizes (n) noted in legends for Figures 4, 6, 7, S1, S6, and S7 refer to the number of biological replicates analyzed. Data were expressed as the mean plus or minus the standard error of the mean (SEM). Statistical analyses were performed using the GraphPadPrism8 software with either the Unpaired Student's t test for two group comparisons, or one-way ANOVA with Dunnett's multiple comparison test for multiple group comparisons. $p < 0.05$ was considered statistically significant. In all figures, asterisks denote statistical significance, where *$p < 0.05$, **$p < 0.01$, ***$p < 0.001$, and ****$p < 0.0001$.